Cosmic-ray acceleration and star formation in the gamma ray SNR RX J1713.7–3946

Yasuo Fukui[1,2]* and Hidetoshi Sano[1,2]

[1]Institute for Advanced Research, Nagoya University, Furo-cho, Chikusa-ku, Nagoya 464-8601, Japan (fukui@a.phys.nagoya-u.ac.jp); [2]Department of Physics, Nagoya University, Furo-cho, Chikusa-ku, Nagoya 464-8601, Japan

Abstract: SNRs are the most probable site where cosmic ray acceleration is verified in the Milky Way. RX J1713.7–3946 is the brightest TeV gamma ray SNR observed by H.E.S.S. and attracted most intensive interest on the origin of cosmic rays (e.g., Aharonian et al. 2006; Fukui et al. 2003). RX J1713.7–3946 is also a unique site of recent star formation as verified by the protostellar outflow and several protostellar infrared sources (Moriguchi et al. 2005; Sano et al. 2010). A recent comparative study between TeV gamma rays and the interstellar hydrogen (HI and H_2) has demonstrated good correspondence between them, supporting the hadronic origin of the gamma rays (Fukui et al. 2012; Inoue et al. 2012). The SNR RX J1713.7–3946 is a top-priority object where cosmic ray acceleration up to the highest energy close to the knee is taking place. Future goals in studying RX J1713.7–3946 include the energy-dependent cosmic ray penetration into the dense HI-H_2 gas and the detection of the lower energy cosmic-ray tail which contributes the ionization of the star forming clumps. In this contribution we will present the state-of-the-art understanding on the cosmic ray acceleration in RX J1713.7–3946 based on the extensive datasets of dense ISM obtained with NANTEN, NANTEN2, ATCA, and H.E.S.S..

SNRs as cosmic ray accelerators

- It is a longstanding question how cosmic-ray (CR) protons, the major constituent of CRs, are accelerated in interstellar space. Supernova remnants (SNRs) are the most likely candidates for acceleration because the high-speed shock waves offer an ideal site for diffusive shock acceleration (DSA; e.g., Bell 1978; Blandford & Ostriker 1978). The principal site of CR proton acceleration is, however, not yet identified observationally in spite of a number of efforts to address this issue.
- Gamma-ray SNRs hold a key to understand the origin of CRs. In particular, young shell- type SNRs (~2000 yrs old) produce gamma-rays via two mechanisms below (see Figure 1).
- If the hadronic process is dominantly working, we expect that the spatial distribution of the gamma-rays corresponds to that of the ISM protons.

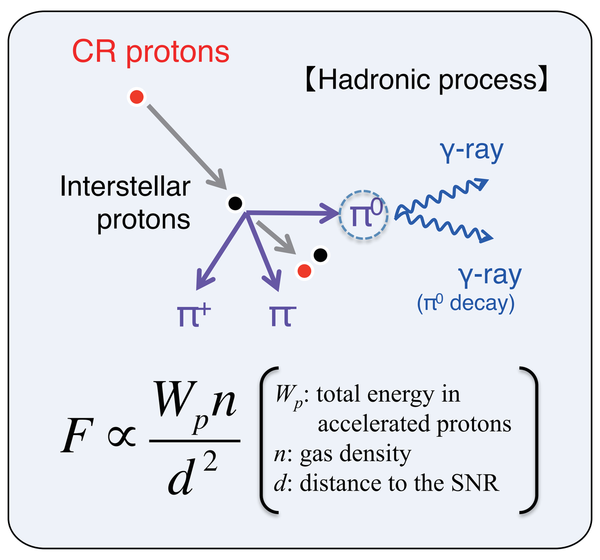

$$F \propto \frac{W_p n}{d^2}$$

W_p: total energy in accelerated protons
n: gas density
d: distance to the SNR

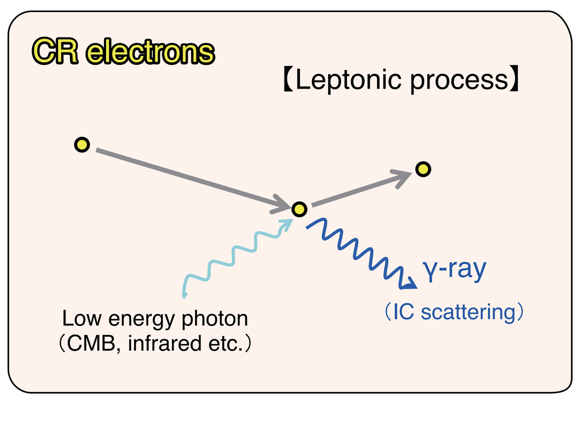

Figure 1: Radiation mechanisms for the hadronic process (left) and the leptonic process (right). CR electrons also emits gamma-rays via non-thermal Bremsstrahlung, but are not dominated in young SNRs.

Young TeV gamma-ray SNR RX J1713.7–3946

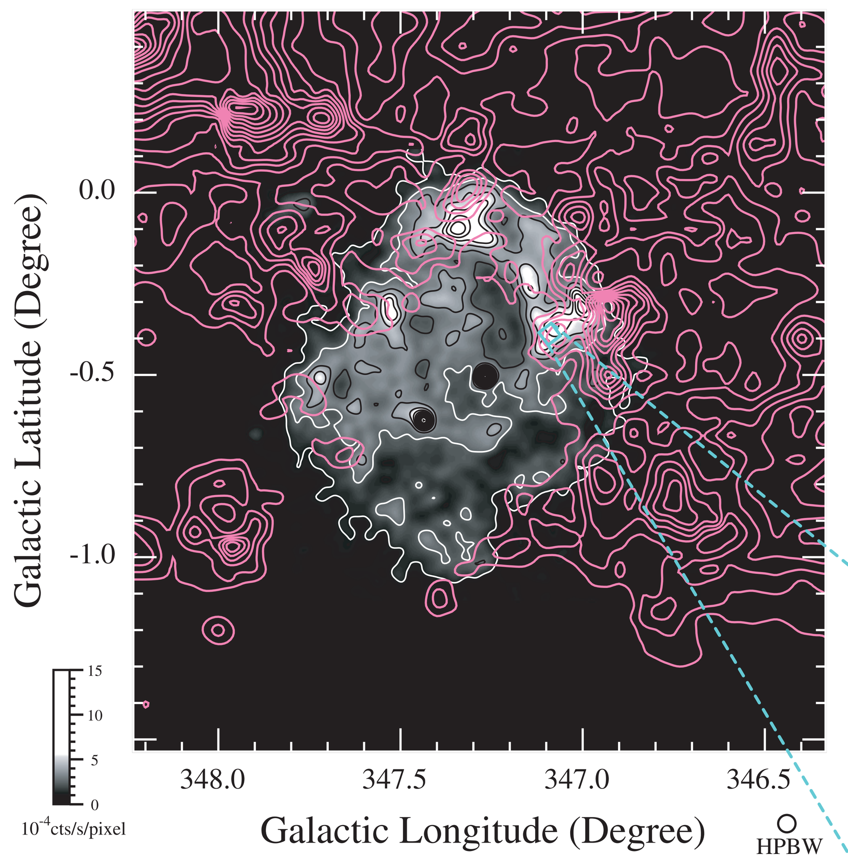

Figure 2: Map of ROSAT synchrotron X-ray image (gray scale) overlaied on the NANTEN2 ^{12}CO(J = 1–0) intensity contours in purple (Fukui et al. 2003). The intensity is derived by integrating the CO spectra from –11 to –3 km s^{-1}, which is considered to be a velocity component inter- acting with the SNR. The lowest contour level and interval of CO are 4 K kms^{-1}.

RX J1713.7–3946 (G347.3–0.5)

- Shell-type & core-collapse SNR
- Discovered by ROSAT [13]
- Distance: ~ 1 kpc [6]
- Diameter: ~ 16.4 pc [6]
- Age: ~ 1600 yr [6,16]
- Bright in both synchrotron X-rays and TeV γ-rays [e.g., 2,3,13]
- Interacting with molecular clouds [e.g., 6,7,12,14]
- Embedded within the star-forming core [12,14]

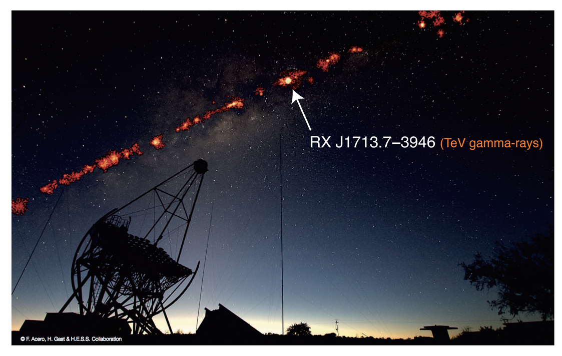

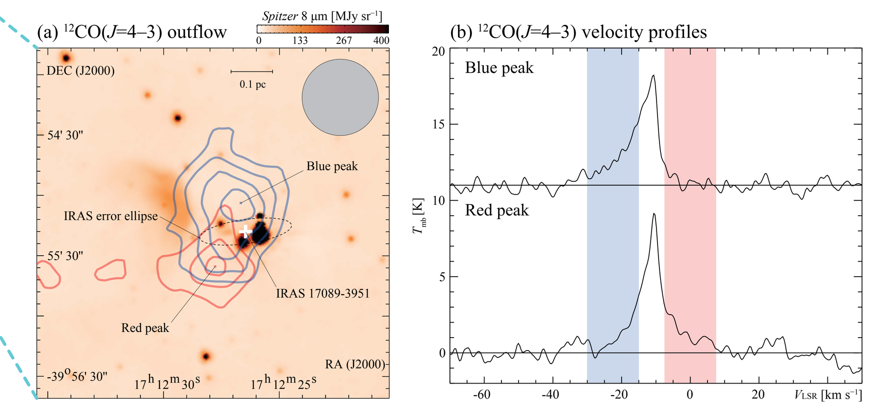

Figure 3: (a) Overlay map RX J1713.7–3946 Spitzer 8 μm image in color scale (from GRIMPS Archive) and ^{12}CO(J = 4–3) intensity contours taken by NANTEN2. The blue con- tours are from –30 to –15 km s^{-1} and the red contours from –8 to 7 km s^{-1}. The lowest contour level of the red and blue contours are 9.6 K km s^{-1} (~4σ) for each. The contour interval of the black contour is 10.2 K km s^{-1} (~3σ), whereas that of the others is 4.8 K km s^{-1} (~2σ). Open cross and enclosed black dashed circle show the positions of the IRAS point source and the 90% confidence region, respectively. (b) ^{12}CO(J = 4–3) spectra covering a velocity range from –70 to 50 km s^{-1}. Areas shaded blue and red correspond to the respective color contours in (a).

Distribution of TeV gamma-rays, CO, and HI

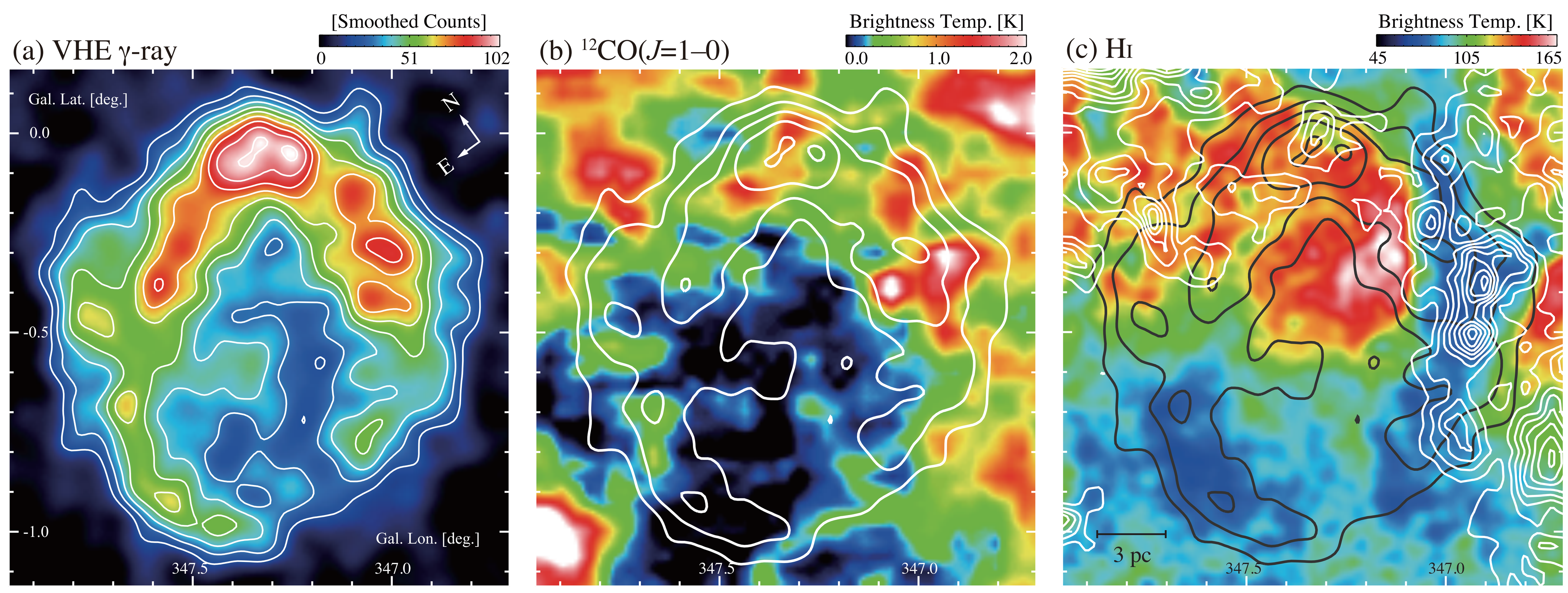

Figure 4: (a) The H.E.S.S. TeV γ-ray distribution of RX J1713.7–3946 in smoothed excess counts above the CR background (Aharonian et al. 2007). Contours are plotted every 10 smoothed counts from 20 smoothed counts. (b) Averaged brightness temperature distribution of ^{12}CO(J = 1–0) emission in a velocity range of V_{LSR} = –20 to 0 km s^{-1} is shown in color (Fukui et al. 2003; Moriguchi et al. 2005). White contours show the H.E.S.S. TeV γ-ray distribution and are plotted every 20 smoothed counts from 20 smoothed counts. (c) Averaged brightness temperature distribution of HI emission obtained by ATCA and Parkes in a velocity range from V_{LSR} = –8 to –6 km s^{-1} (McClure-Griffiths et al. 2005) is shown in color. White contours show the ^{12}CO(J = 1–0) brightness temperature integrated in the same velocity range every 1.0 K km s^{-1} (~3σ).

- The general ^{12}CO(J = 1–0) distribution is shell-like associated with the γ-ray shell, showing weaker or no CO emission in part of the south.
- We find dark HI clouds of around 60 K in the west and in the southeast.
- These dark HI clouds are not due to absorption of the radio continuum radiation which is very weak toward the SNR (Lazendic et al. 2004).

Optically thick HI cloud

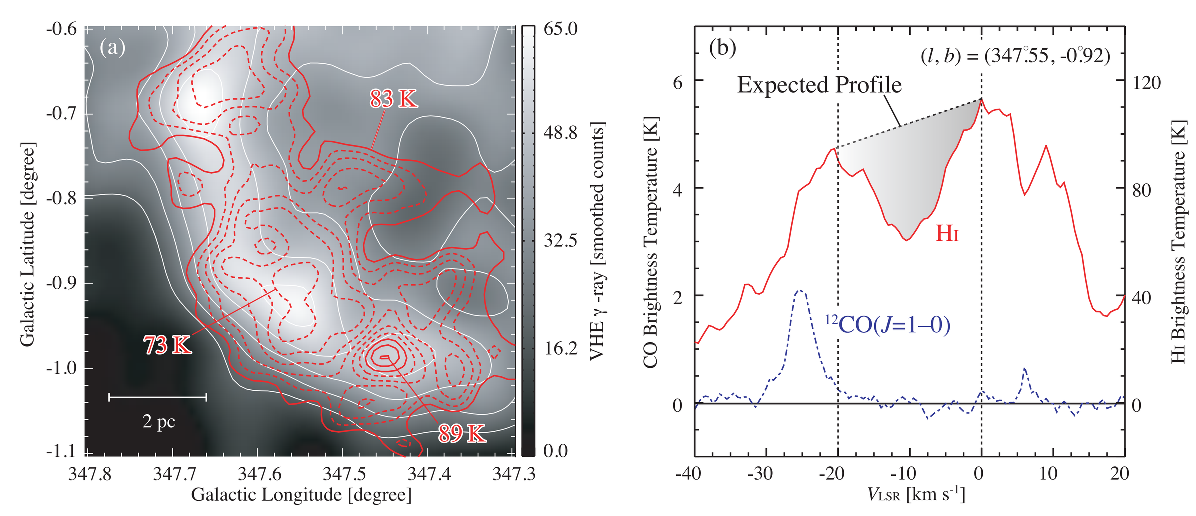

Figure 5: (a) The H.E.S.S. TeV γ-ray distribution toward the SE cloud (Aharonian et al. 2007). Red contours show the averaged HI brightness temperature distribution in a velocity range from –15 to –5 km s^{-1} (McClure-Griffiths et al. 2005). (b) The HI and ^{12}CO(J = 1–0) spectra at (l, b) = (347.55, –0.92). The shaded area shows an expected HI profile.

- The dark HI region, the SE cloud, shows no CO, and we suggest that its density is lower and its T_s is higher than that in the CO W cloud. HI brightness $T_L(V)$ is expressed as follows (e.g., Sato & Fukui 1978):

$$T_B(v) = T_s[1 - e^{-\tau(v)}] + T_{BG}(v)e^{-\tau(v)}$$

- We estimate the absorbing dark HI column density to be N_p(HI) = 1.0 × 10^{21} cm^{-2} (optical depth = 0.8), 1.8 × 10^{21} cm^{-2} (optical depth = 1.1), and 3.1 × 10^{21} cm^{-2} (optical depth = 1.5) for three assumed cases T_s = 30, 40, and 50 K, respectively, for the half-power width Δv=10 km s^{-1}, where the HI optical depth τ is estimated by Equation (2) and N_p(HI) by the following relationship:

$$N_p(\mathrm{HI}) = 1.823 \times 10^{18}\, T_s\, \Delta v\, \tau\ [\mathrm{cm}^{-2}]$$

Total ISM protons

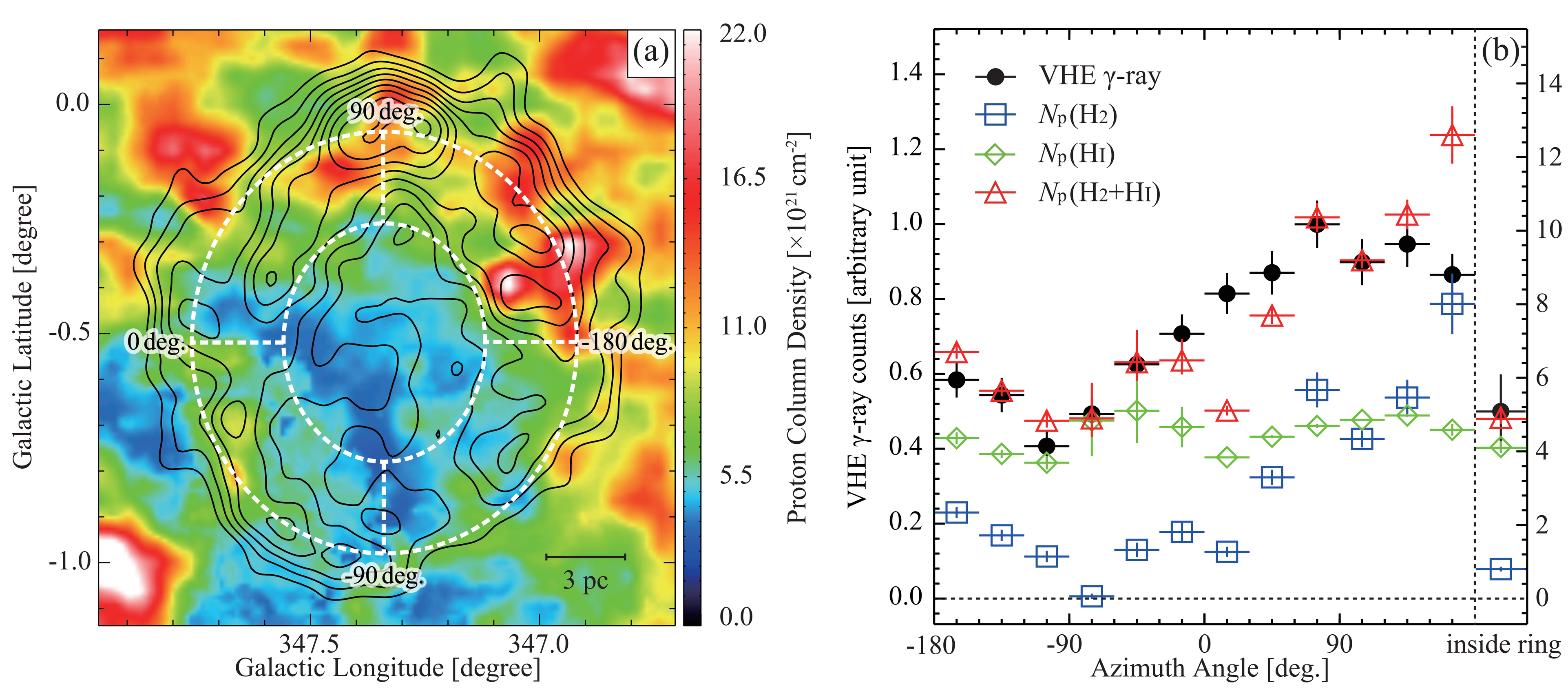

Figure 6: . (a) Distributions of column density of the total ISM protons N_p(H_2 + HI) in a velocity range from –20 to 0 km s^{-1}. Contours are the same as in Figure 4(a). (b) Azimuthal distributions of N_p(H_2), N_p(HI), N_p(H_2 + HI), and TeV γ-ray-smoothed counts per beam between the two elliptical rings shown in (a). The proton column densities are averaged values between the rings. Semimajor and semiminor radii of the outer ring are 0.46 degree and 0.42 degree, respectively, and the radii of the inner ring are half of them. The same plots inside the inner ring are shown on the right side of (b).

- The total ISM proton density N_p(H_2+HI) shows good agreement with the γ-ray angular distribution and the central part in the inner ring.
→ An observational evidence for the hadronic gamma-ray (= cosmic-ray protons are accelerated by the SNR)
- The total mass of the ISM protons responsible for the γ-rays is 2.0 × 10^4 $M_\odot$ over the whole SNR (radius 0.65 degree); the mass of molecular protons is 0.9 × 10^4 $M_\odot$ and that of atomic protons is 1.1 × 10^4 $M_\odot$, where we assume that the ISM protons interacting with the CR protons is proportional to the TeV γ-rays. The total cosmic-ray proton energy is calculated to be ~(0.8–2.3) × 10^{48} erg.

Discussion & Summary

- We have shown that a cobined analysis of CO and HI provides a reasonable candidate for the target ISM protons and thereby lends new support to the hadronic scenario.
- We argue here that the highly inhomogeneous distribution of the ISM, the cavity, and the dense and clumpy wall opens up the possibility of accommodating the low-density site for DSA and the high-density target simultaneously as discussed into detail by Inoue et al. (2012, see also Fig. 7c).
- The hard *Fermi*-LAT GeV spectrum is also explained well by the hadronic scenario being due to the energy-dependent penetration of CR protons into the dense clouds and that the leptonic scenario explaining the spectrum is not unique.

The penetration depth of CRs (Inoue et al. 2012) $l_{pd} = 0.1\,\eta^{1/2}\left(\frac{E}{10\ \mathrm{TeV}}\right)^{1/2}\left(\frac{B}{100\ \mu\mathrm{G}}\right)^{-1/2}\left(\frac{t_{age}}{10^3\ \mathrm{yr}}\right)^{1/2}$ pc

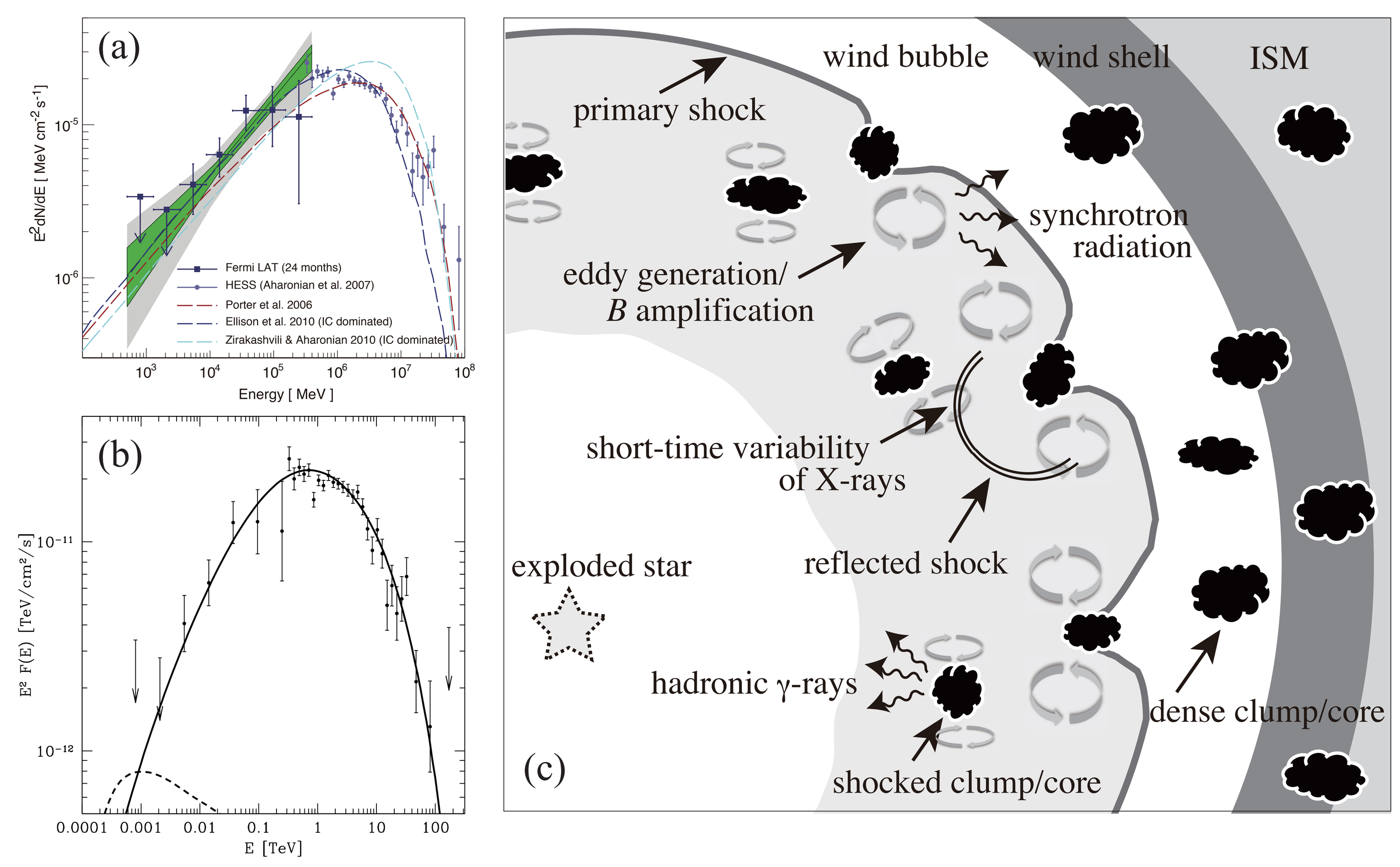

Figure 7: . (a) Leptonic gamma-rays from RX J1713.7–3946 (Abdo et al. 2011). Shown is the Fermi-LAT-detected emission in combination with the energy spectrum detected by H.E.S.S.. The green region shows the uncertainty band obtained from our maximum likelihood fit of the spectrum. The gray region depicts the systematic uncertainty of this fit obtained by variation of the background and source models. The black error bars correspond to independent fits of the flux of RX J1713.7–3946 in the respective energy bands. Also shown are curves that cover the range of models proposed for this object. (b) Hadronic gamma-rays from RX J1713.7–3946 (Gabici & Aharonian 2014). The emission from the clumps is shown as a solid line, while the dashed line refers to the emission from the diffuse gas in the shell. Data points refer to Fermi and HESS observations. (c) Schematic picture of the shock–cloud interaction model (Inoue et al. 2012).

References

[1] Abdo et al. 2011, ApJ, 734, 28 [2] Aharonian et al. 2006, A&A, 449, 223 [3] Aharonian et al. 2007, A&A, 464, 235 [4] Bell 1978, MNRAS, 182, 147 [5] Blandford & Ostriker 1978, [6] Fukui et al. 2003, PASJ, 55, 61 [7] Fukui et al. 2012, ApJ, 746, 82 [8] Gabici & Aharonian 2014, MNRAS, 445, 70 [9] Inoue et al. 2012, ApJ, 744, 71 [10] Lazendic et al. 2004, ApJ, 602, 271 [11] McClure-Griffiths et al. 2005, ApJS, 158, 178 [12] Moriguchi et al. 2005, ApJ, 631, 947 [13] Pfeffermann & Aschenbach 1996, rftu, 267 [14] Sano et al. 2010, ApJ, 724, 59 [15] Sato & Fukui 1978, AJ, 83, 1607 [16] Wang et al. 1997, A&A, 318, 59